FIGNL1-FIRRM is essential for meiotic recombination and prevents DNA damage-independent RAD51 and DMC1 loading
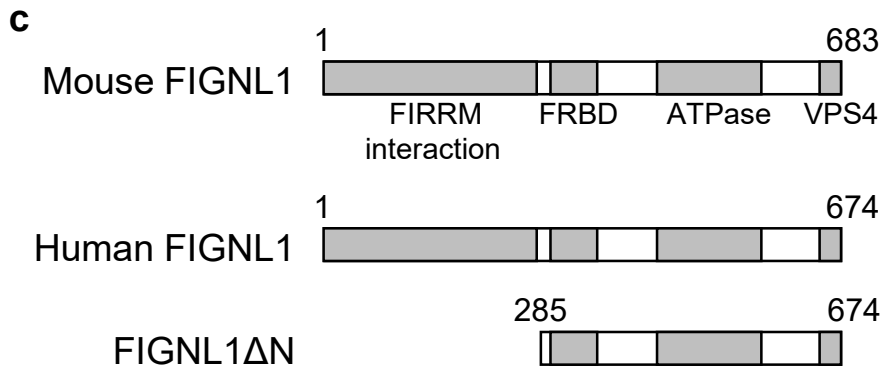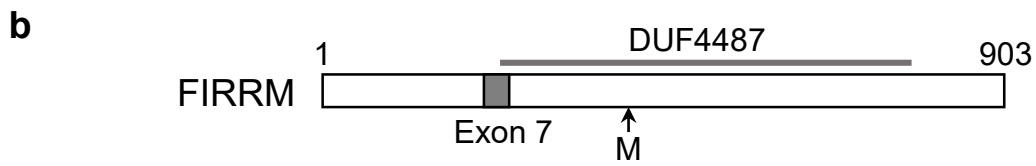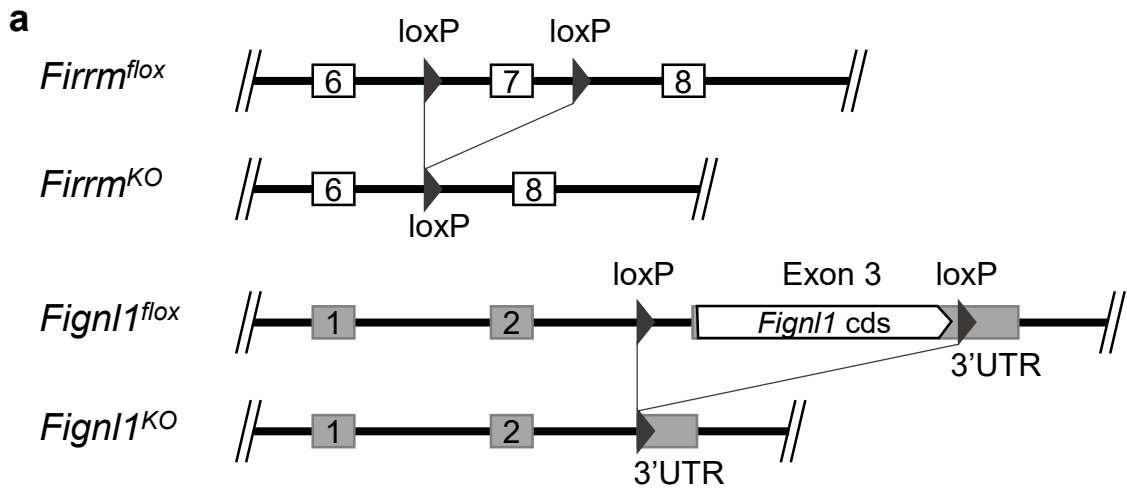
Akbar Zainu, Pauline Dupaigne, Soumya Bouchouika, Julien Cau, Julie A. J. Clément, Pauline Auffret, Virginie Ropars, Jean-Baptiste Charbonnier, Bernard de Massy, Raphael Mercier, Rajeev Kumar, Frédéric Baudat
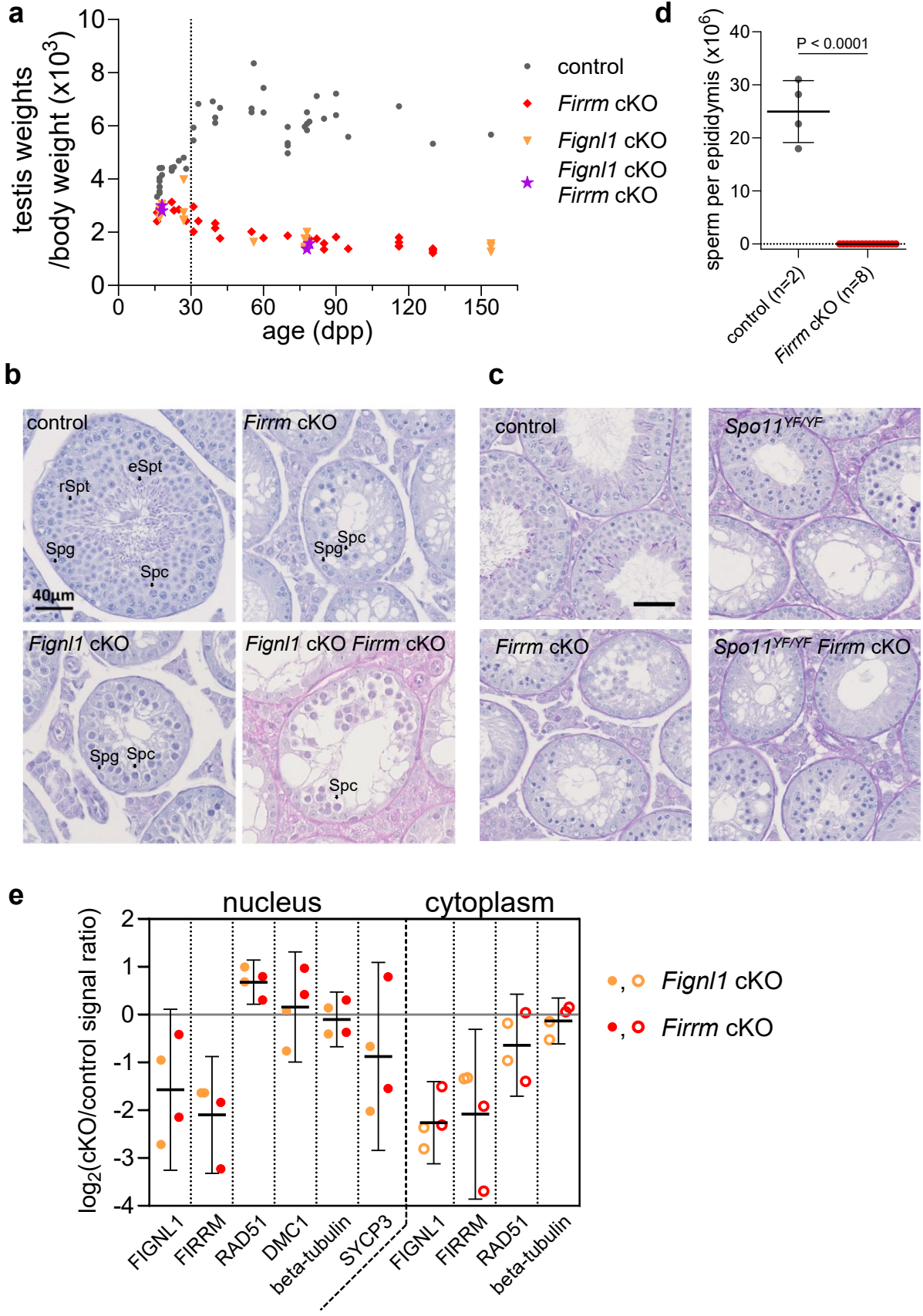
Supplementary figures 1-9
Supplementary tables 1-2

Supplementary Figure 1

a

b

c

Supplementary Fig. 1. Structure of *Firrm* and *Fignl1* cKO alleles. a. Genomic structure of the floxed and knockout (KO) *Firrm* and *Fignl1* alleles. Open boxes, coding exons; gray-filled boxes, non-coding exons**. b.** The mouse FIRRM protein. The conserved DUF4487 domain is indicated, with the position of exon 7 deleted in the KO (generating a frameshift), and the following internal methionine (M, position 406). **c.** Domain organization of mouse (683aa) and human (674aa) FIGNL1 proteins and the human FIGNL1ΔN truncation mutant. Source data are provided as a Source Data file.

**Supplementary Fig. 2. Spermatogenesis is defective in *Firrm* cKO and *Fignl1* cKO mice. a.** Testis weight relative to body weight in control (gray, n=44), *Firrm* cKO (red, n=24), *Fignl1* cKO (orange, n=18) and *Firrm* cKO *Fignl1* cKO (purple, n=4) mice of various ages (16 dpp to 154 dpp). Data from 30 dpp (dotted line) or older individuals were plotted in Fig. 1a. **b-c.** Periodic acid-Schiff-stained testis sections from 10-11-week-old **(b)** or 8-week-old **(c)** mice of the indicated genotypes. Note the depletion of germ cells in 10-11-week-old *Firrm* cKO, *Fignl1* cKO and *Firrm* cKO *Fignl1* cKO tubules, as well as in 8-week-old *Firrm* cKO (and *Spo11*$^{YF/YF}$ *Firrm* cKO) compared to *Spo11*$^{YF/YF}$ tubules. Spg, spermatogonia; Spc, spermatocytes; rSpt, round spermatids; eSpt, elongated spermatids. Scale bar, 40 µm **(b)** or 50 µm **(c)**. **d.** Sperm count in cauda epididymis from 4-month-old mice (Mean ± SD, unpaired t-test). **e.** Quantification of the western blot signal of cytoplasmic (80µg) and nuclear (100µg) fractions from testes of 12 dpp mice of the indicated genotypes (n=2 independent extracts from 3-4 mice per genotype). The log$_2$ of *Fignl1 cKO* (orange) or *Firrm cKO* (red) over control signal ratio is shown. Black bar, geometric mean with 95% confidence interval of pooled data from *Fignl1* cKO and *Firrm* cKO experiments. Source data are provided as a Source Data file.

Supplementary Figure 3

a

| | Pre-Leptotene | Early Leptotene | Mid-late Leptotene | Early Zygotene | Mid Zygotene | Late Zygotene |

control: RAD51, DMC1, SYCP3/RAD51/DMC1

Firrm cKO: RAD51, DMC1, SYCP3/RAD51/DMC1

b

SYCP3 | TEX11 | SYCP3 TEX11

control

Firrm cKO

c

MSH4 foci per nucleus vs SC length (μm)

- control
- *Firrm* cKO
- *Spo*^{YF/YF}*Firrm*cKO
- *Spo*^{YF/YF}

d

off-axis RPA2 foci

Pre-Leptotene: ns, ns, ns
Early Leptotene: *, ****, ****
Mid-late Leptotene: ns, *, ****
Early Zygotene: *, ns, ***
Mid Zygotene: ***, ns, ***
Late Zygotene: ns, *, ****

control, *Firrm* cKO, *Fignl1* cKO

e

RPA2 and RAD51 colocalization in preleptotene nuclei

number of foci per nucleus / number of foci

control: RAD51, RPA (Total); RAD51 obs, RAD51 random, RPA obs, RPA random (Coloc.) — ***, ***

Fignl1 cKO: RAD51, RPA (Total); RAD51 obs, RAD51 random, RPA obs, RPA random (Coloc.) — ****, ****

Supplementary Fig. 3. Increased RAD51 and DMC1 loading, and defective MSH4 and TEX11 focus formation, in *Firrm* cKO and *Fignl1* cKO spermatocytes. a. Representative images of preleptotene to late zygotene spermatocyte spreads from control and *Firrm* cKO mice stained for SYCP3, RAD51 and DMC1. Scale bar, 10 μm. **b.** Spreads of zygotene spermatocytes from 16 dpp control and *Firrm* cKO mice stained with SYCP3 and TEX11. **c.** Number of MSH4 foci along SYCP1-marked synaptonemal complex fragments in control (gray), *Firrm* cKO (red), *Spo11*$^{YF/YF}$ *Firrm* cKO (purple), and *Spo11*$^{YF/YF}$ (blue) zygotene or zygotene-like spermatocytes. The number of MSH4 foci varied with the SC length in control and *Firrm* cKO spermatocytes. The linear regression fit is shown, with the standard error. **d.** Numbers of off-axis RPA2 foci in control (gray), *Firrm* cKO (red) and *Fignl1* cKO (orange) spermatocytes. Same mice as in Fig. 2d. **e.** Numbers of all and of colocalized RAD51 (green) and RPA2 (red) foci in spreads of preleptotene control and *Fignl1* cKO spermatocyte nuclei. n=2 (control) or n=3 mice (*Fignl1* cKO). The numbers of observed and expected by chance (random) colocalized foci are shown (see Methods). Wilcoxon two-tailed test. Source data are provided as a Source Data file.
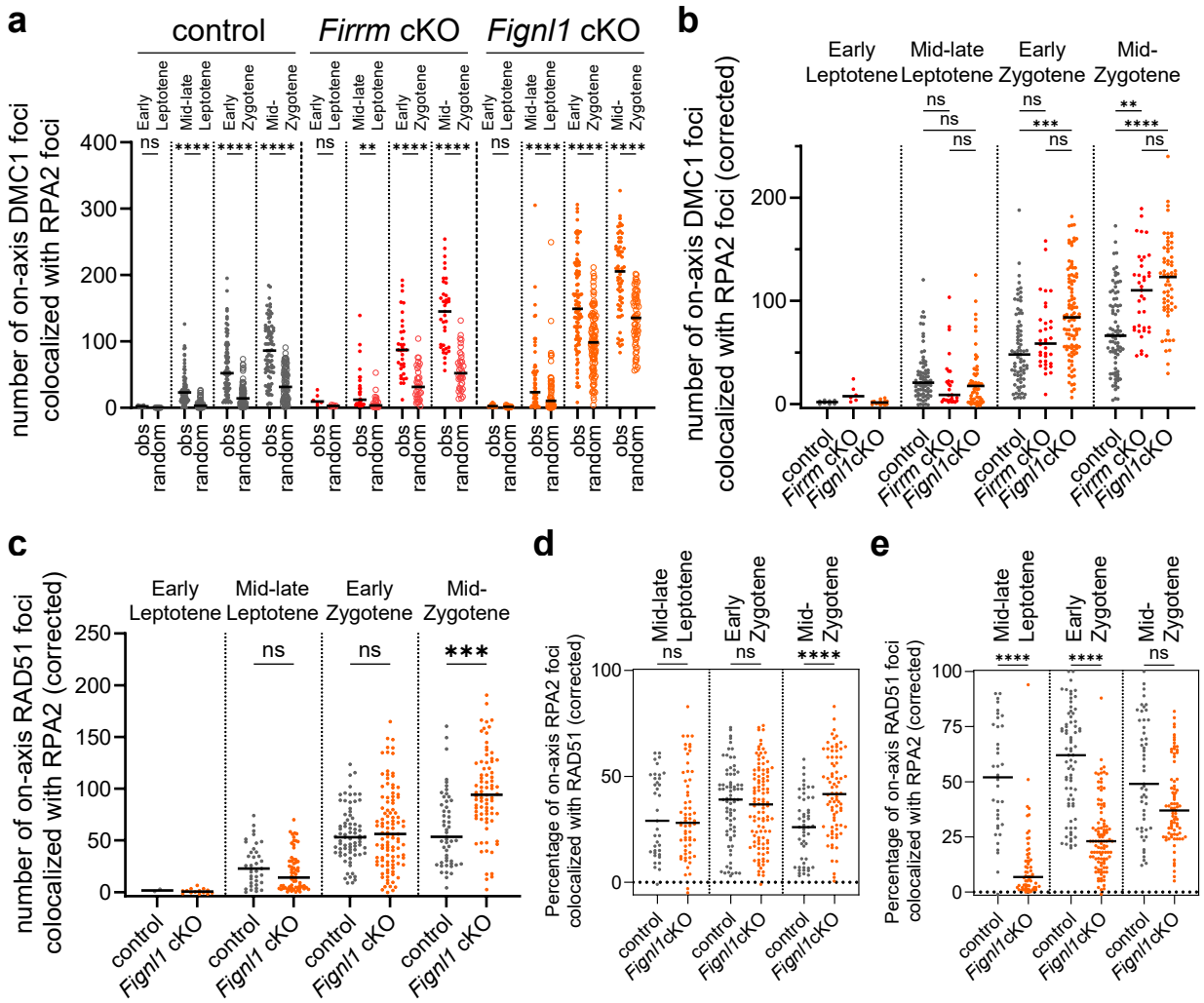
Supplementary Figure 4
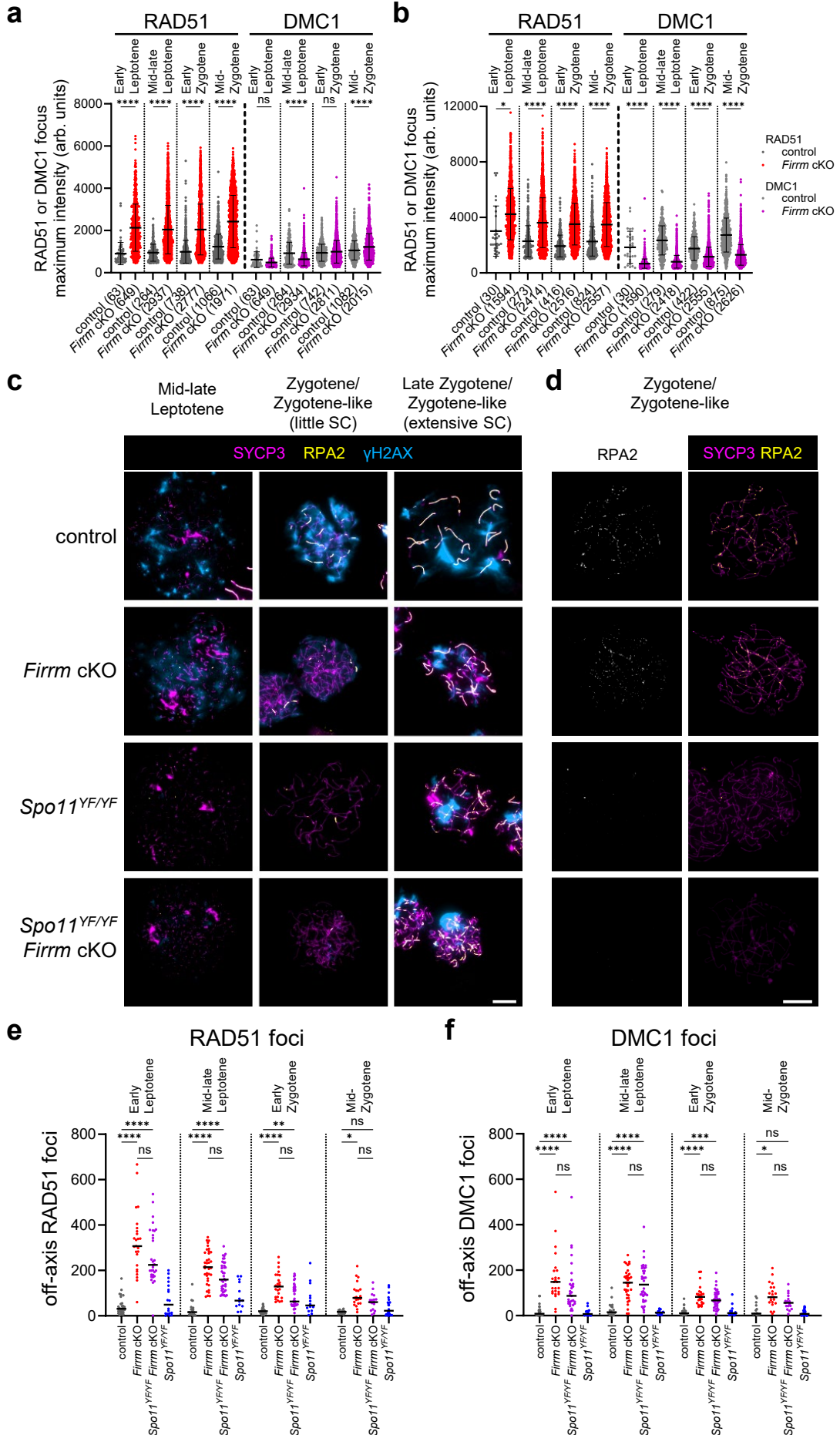
Supplementary Fig. 4. Absence of meiotic DSBs, but presence of RAD51 and DMC1 off-axis foci, in *Spo11*^YF/YF^ ***Firrm* cKO spermatocytes. a-b.** Intensity of RAD51 and DMC1 foci in spread spermatocytes from control (RAD51, dark gray; DMC1, light gray) and *Firrm* cKO (RAD51, red; DMC1, purple) 12 dpp mice (replicate 1 **(a)** and replicate 2 **(b)**, n=1 mouse per genotype per replicate) co-stained for RAD51 and DMC1 (guinea-pig primary antibody). Only co-localized foci were considered. The mean ± SD is shown. Two-sided Dunn's multiple comparison tests. **c-d.** Representative spread nuclei of spermatocytes from control, *Firrm* cKO, *Spo11*^YF/YF^ *Firrm* cKO, and *Spo11*^YF/YF^ mice stained for SYCP3, SYCP1 and γH2AX **(c)** or for SYCP3 and RPA2 **(d)**. Scale bar, 10 μm. **e-f**. Numbers of off-axis RAD51 **(e)** and DMC1 **(f)** foci for control (gray), *Firrm* cKO (red), *Spo11*^YF/YF^ *Firrm* cKO (purple), and *Spo11*^YF/YF^ (blue) spermatocyte spreads. Source data are provided as a Source Data file.

Supplementary Figure 5
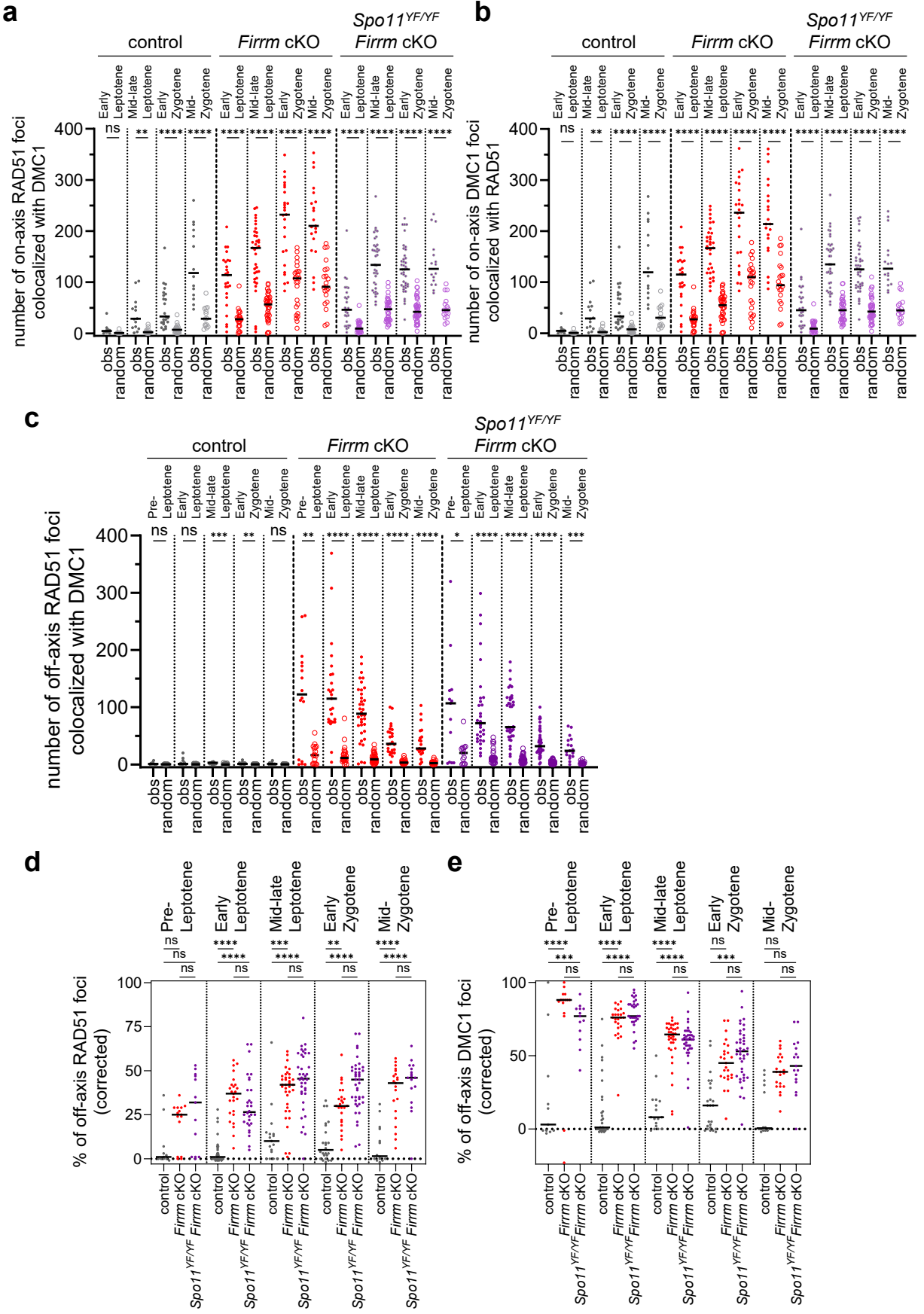
Supplementary Fig. 5. SPO11 DSB-independent DMC1 and RAD51 foci colocalize in *Spo11^{YF/YF} Firrm* cKO spermatocytes. a-b. Number of on-axis RAD51 foci colocalized with on-axis DMC1 foci **(a)**, and vice-versa **(b),** on spread from spermatocytes of 12 dpp mice of the indicated genotypes. n=2 mice per genotype. Two-sided Sidak's multiple comparison tests. **(a-e)**. **c-e**. Number **(c)** or percentage (corrected for random colocalization) **(d-e)** of off-axis RAD51 foci colocalized with off-axis DMC1 foci **(c-d)**, and vice-versa **(e)**. Two-sided Sidak's multiple comparison tests **(c)** or two-sided Dunn's multiple comparison tests **(d-e)**. Source data are provided as a Source Data file.
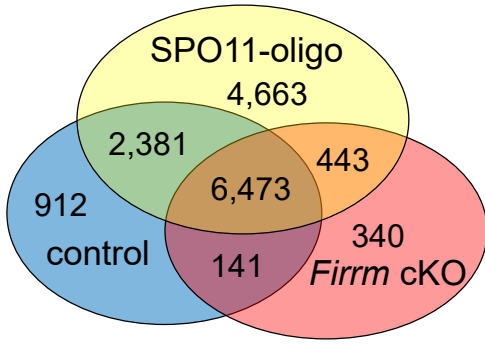
Supplementary Figure 6

Supplementary Fig. 6. Similar numbers of DMC1 and RPA2 foci colocalize in wild-type and *Firrm* cKO spermatocytes. a-b. Number of on-axis DMC1 foci colocalized with on-axis RPA2 foci on spreads from spermatocyte nuclei from control, *Firrm* cKO and *Fignl1* cKO mice. The observed (obs) and expected by chance (random) numbers of DMC1 foci colocalized with RPA2 are shown in **(a)**, while the counts are corrected for the number expected by chance in **(b)**. obs, number of detected colocalizing foci. Random, average of 100 simulations where the colocalization of randomly distributed DMC1 foci with actual RPA2 foci was measured. **c-e.** Number **(c)** and percentages **(d-e)** of on-axis RAD51 foci colocalized with on-axis RPA2 foci on spreads from spermatocyte nuclei from control (n=2) and *Fignl1* cKO (n=3) mice. The counts corrected for the number expected by chance are shown in **(c)**. **d, e.** Percentage (corrected for random colocalization) of RPA2 foci colocalized with RAD51 **(d)** and vice-versa **(e)**. Two-sided Sidak's multiple comparison tests **(a)** or two-sided Dunn's multiple comparison tests **(b-e)**. Source data are provided as a Source Data file.
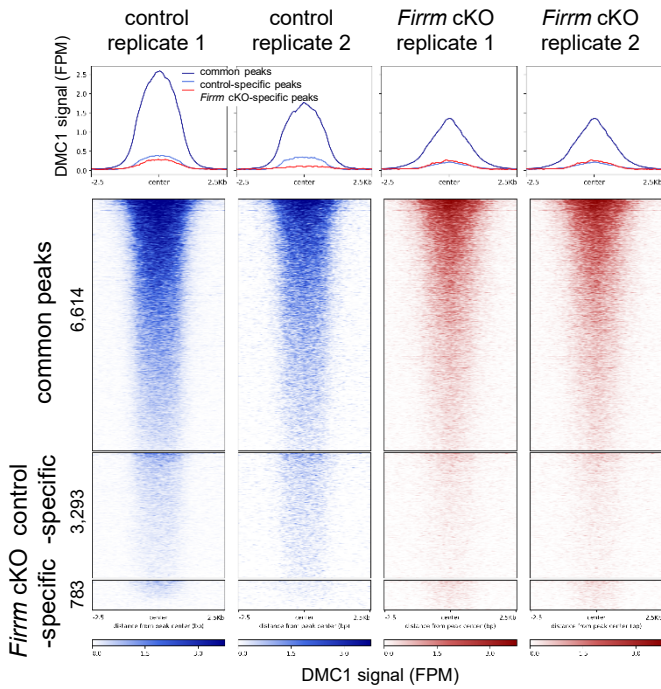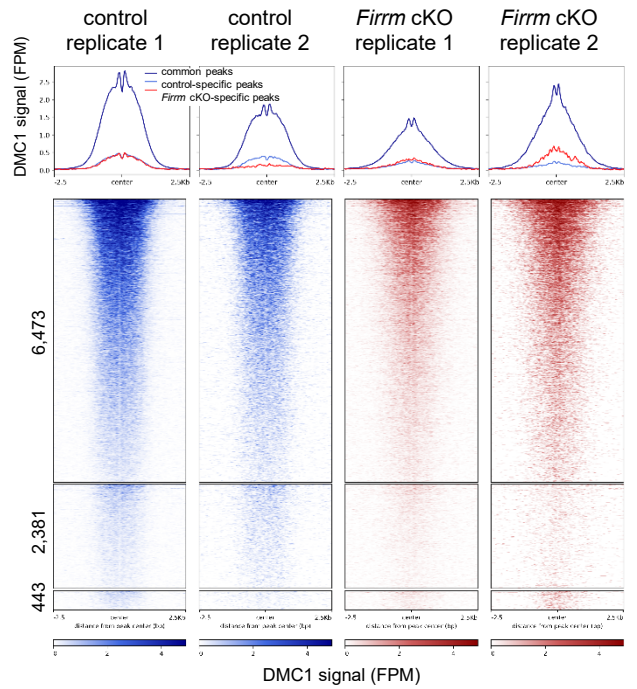
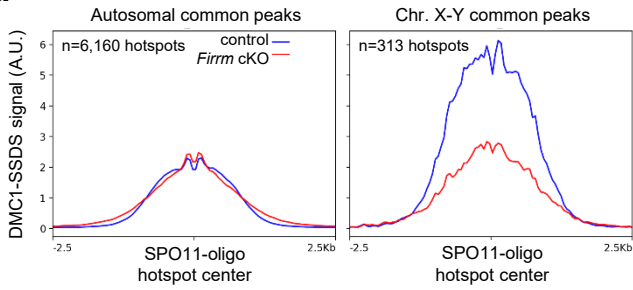# Supplementary Figure 7

a
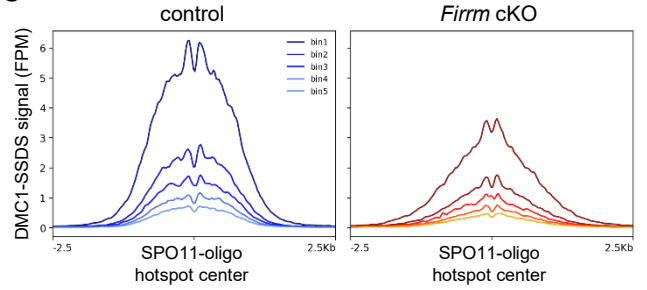

b

All peaks

c

Peaks overlapping SPO11-oligo hotspots,
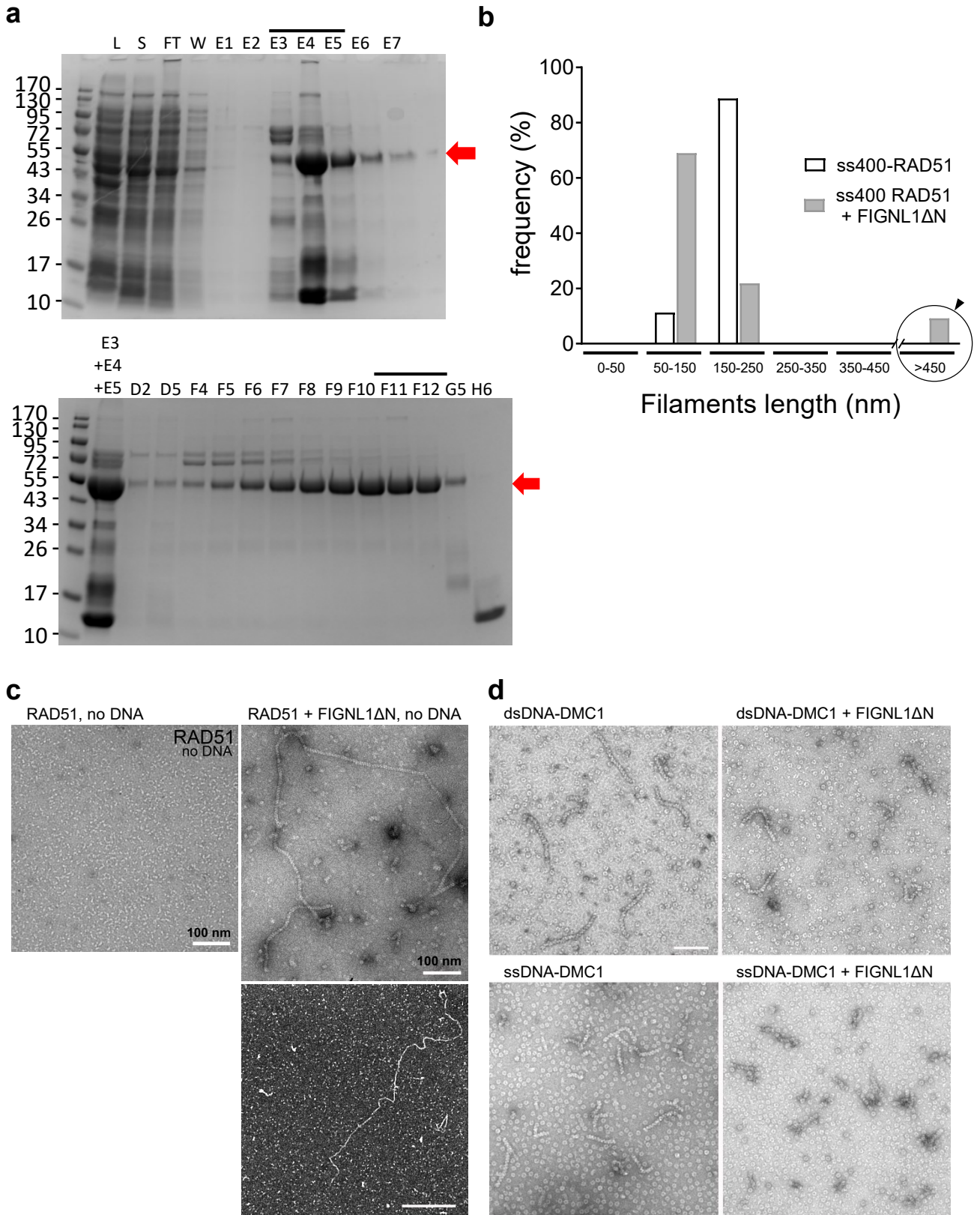centered to SPO11-oligo hotspot center

d

e

Supplementary Fig. 7. DMC1 recruitment at meiotic DSB hotspots in *Firrm* cKO spermatocytes. a.
Numbers and overlap of hotspots identified by DMC1-SSDS in spermatocytes from 12 dpp control and
Firrm cKO mice, and of SPO11-oligo hotspots detected in C57BL/6J mice in [77]. **b-c**. Average plots (top)
and corresponding heatmaps (bottom) of DMC1-SSDS signal in control and *Firrm* cKO mice (2 biological
replicates/each), at all common, control-specific, and *Firrm* cKO-specific DMC1 hotspots identified in
our analysis **(b)**, and at hotspots overlapping with SPO11-oligo hotspots detected in C57BL/6J mice **(c)**.
In **(c)**, the center of the intervals was the center of SPO11-oligo peaks detected in B6 mice, as defined
in (Lange, 2016). **d.** Average DMC1-SSDS signal distribution at common DMC1 hotspots, defined in **(c)**,
at autosomal hotspots (left panel) and at X and Y chromosome hotspots (right panel), for control (blue)
and *Firrm* cKO (red). The DMC1-SSDS signal was normalized to have the same total amount of
normalized signal for all common hotspots (on 5-kb windows) in both genotypes. The relative excess
of DMC1-SSDS signal at X-Y chromosome hotspots in control is clear. **e.** Average plots of DMC1-SSDS
signal intensity (in FPM) at common hotspots as defined in **(c)**, ranked within 5 bins of decreasing
intensity.

Supplementary Figure 8
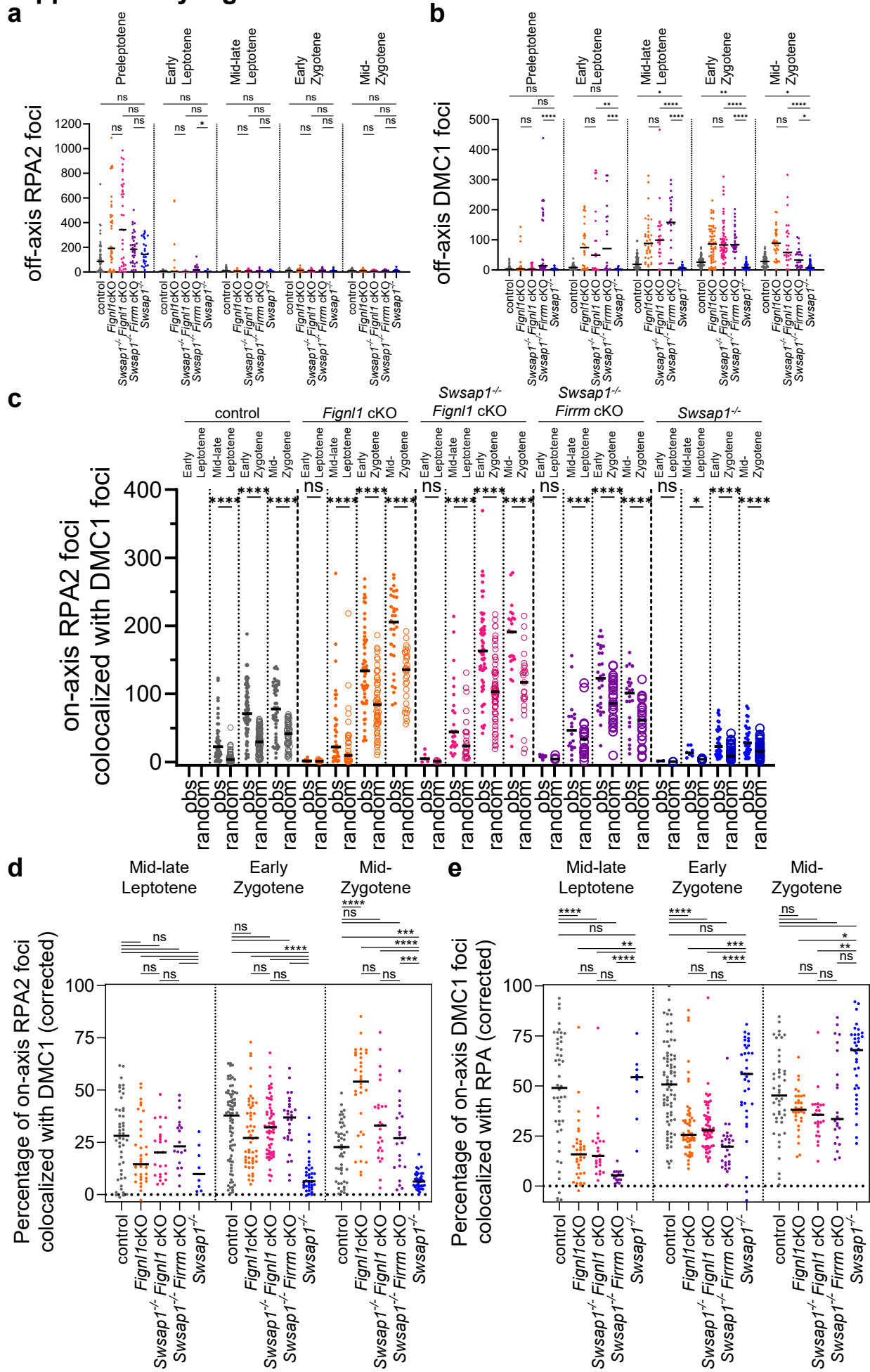
Supplementary Fig. 8. *Fignl1* **deletion restores the formation of DMC1 foci in** *Swsap1*^{-/-} **spermatocytes. a-b.** Numbers of off-axis RPA2 **(a)** and DMC1 **(b)** foci detected on spermatocyte spreads from 17 dpp control mice of the indicated genotypes. n=1-3 mice per genotype (see legend of Fig. 7). **c-e.** Numbers **(c)** or percentages **(d,e)** of on-axis RPA2 foci colocalized with on-axis DMC1 foci **(c,d)** or vice-versa **(e)** in spermatocyte spreads from 17 dpp mice. The numbers of colocalized foci were corrected to the number expected by chance (see Methods). Two-sided Sidak's multiple comparison tests **(c)** or two-sided Dunn's multiple comparison tests **(a,b,d,e)**. Source data are provided as a Source Data file.

a

b

c

RAD51, no DNA

RAD51 + FIGNL1ΔN, no DNA

d

dsDNA-DMC1

dsDNA-DMC1 + FIGNL1ΔN

ssDNA-DMC1

ssDNA-DMC1 + FIGNL1ΔN

Supplementary Fig. 9. FIGLN1 alters the architecture and the activity of RAD51 and DMC1 nucleoprotein filaments. a. Purification of recombinant Histidine-tagged human FIGNL1ΔN284 protein from *E. coli*. Top panel, SDS-page analysis of proteins in total protein lysate (L), soluble protein fraction (S), flow-through (FT) from Hi-trap column, wash, and elution fractions (E1 to E7). Bottom panel, SDS-PAGE analysis of protein fractions collected during the gel filtration purification. Fractions E3, E4, and E5 from previous step were pooled and are shown as input control. Red arrows indicate recombinant His-FIGNL1ΔN284 with an expected size of 46kDa. F11 and F12 fractions were used for biochemical assays in this study. **b.** Length distribution of RAD51 filaments formed on 400 nt ssDNA fragments without (ss400-RAD51) or with (ss400-RAD51+ FIGNL1ΔN) 1.6 µM human FIGNL1ΔN. Note the presence of >450nm-long filaments when FIGNL1ΔN is present that were not included in the quantification shown in Figure 8f. **c.** Representative TEM images of RAD51 in the presence of ATP but in the absence of DNA (negative staining, left), and in presence of human FIGNL1ΔN (negative staining, scale bar 100nm, top right panel; and positive staining, scale bar 500nm, bottom panel). Note the presence of long filaments despite the absence of DNA. **d.** Representative TEM images (negative staining) of DMC1 filaments assembled on a 400 bp dsDNA (top) or 400 nt ssDNA (bottom) fragment, without (left) or with human FIGNL1ΔN (right). Scale bar, 100 nm. Source data are provided as a Source Data file.

Supplementary Table 1. Primers used for mouse genotyping

Primer	Sequence (5'-3')	Genotype: amplicon
Firrm wild-type and floxed allele, forward	CTTGGCTCGCTTTGCTTTGA	WT: 304bp
Firrm wild-type and floxed allele, reverse	TGTAGTTTACATCTTCCCTATGACA	*Firrm^{fl}*: ~500bp
		Firrm$^-$: -
Firrm floxed and deleted allele, forward	AAGGCGCATAACGATACCAC	WT: -
Firrm floxed and deleted allele, reverse	ACTGATGGCGAGCTCAGACC	*Firrm^{fl}*: ~1kb
		Firrm$^-$: 178bp
Fignl1 wild-type and floxed allele, forward	GGGATCAAACACTAGGGTTCAGGC	WT: 200bp
Fignl1 wild-type and floxed allele, reverse	GATACAGTCTTCAAGATTAAGGACAACC	*Fignl1^{fl}*: 400bp
		Fignl1$^-$: -
Fignl1 deleted allele, forward	GGGATCAAACACTAGGGTTCAGGC	WT: -
Fignl1 deleted allele, reverse	CGGGTTACGGTAGTTTACTCCC	*Fignl1^{fl}*: -
		Fignl1$^-$: 412bp
Stra8-Cre transgenic allele, forward	GTGCAAGCTGAACAACAGGA	No transgene: -
Stra8-Cre transgenic allele, reverse	AGGGACACAGCATTGGAGTC	*Stra8-Cre*: ~150bp
Cmv-Cre transgenic allele, forward	TGGGCGGCATGGTGCAAGTT	No transgene: -
Cmv-Cre transgenic allele, reverse	CGGTGCTAACCAGCGTTTTC	*Cmv-Cre*: 466bp
Spo11 wild-type and YF allele, forward	CTGGTCGATGCAGATCCCTACGG	WT: 394bp
Spo11 wild-type and YF allele, reverse	TAGATGCACATTATCTCGATGCC	*Spo11^{YF}*: 482bp
Swsap1 wild-type and deleted allele, forward	TCTGTGAACTATAGCCAATGAGGC	WT: 396bp
Swsap1 wild-type and deleted allele, reverse	AACTGTCACTCAGGCGCGAACTAG	*Swsap1$^-$*: 265bp

Supplementary Table 2. List of antibodies used in this study

Antibody	Source	Identifier/Reference	Application	Dilution
Guinea-pig anti-SYCP3	home made	DOI: 10.1371/journal.pbio.1000035	IF, WB	1:500, 1:3000
Mouse anti-SYCP3	Abcam	ab97672	IF	1:200
Rabbit anti-SYCP1	Abcam	ab15090	IF	1:400
Mouse anti-γH2AX	Millipore	05-636-I	IF	1:10000
Guinea-pig anti-SYCP1	from H. Cook		IF	1:200
Rabbit anti-MSH4	Abcam	ab58666	IF	1:200
Rabbit anti-RPA2	Abcam	ab76420	IF	1:200
Rat anti-RPA2	Cell Signaling	2208	IF	1:200
Rabbit anti-DMC1	Santa Cruz	sc-22768	IF, WB	1:200, 1:1000
Guinea-pig anti-DMC1	from Prof. Qinghua Shi	DOI: 10.1016/j.molcel.2020.06.015	IF	1:100
Goat anti-DMC1	Santa Cruz	sc-8973	ChIP	
Mouse anti-DMC1	Abcam	ab11054	IF	1:100
Rabbit anti-RAD51	Calbiochem	PC130	IF, WB	1:500, 1:1000
Rabbit anti-FIGNL1	Proteintech	17604-1-AP	WB	1:500
Rabbit anti-C1orf112 (anti-human FIRRM)	Abnova	PAB21606	WB	1:500
Rabbit anti-beta Tubulin	Abcam	ab6046	WB	1:3000
Goat anti-rabbit A488	Molecular Probes	A-21206	IF	1:400
Goat anti-rabbit A555	Molecular Probes	A-21248	IF	1:400
Goat anti-rabbit Star Orange	Abberior GMBH	STORANGE-1002-5	IF -STED	1:100
Goat anti-guinea pig Cy3	Jackson	706-165-148	IF	1:400
Goat anti-guinea pig Cy5	Jackson	706-175-148	IF	1:400
Goat anti-guinea pig Star Red	Abberior GMBH	STRED-1006-500U	IF-STED	1:100
Donkey anti-rat A555	ThermoFisher	A48270	IF	1:400
Goat anti-rat Star Red	Abberior GMBH	STRED-1007-500U	IF-STED	1:100
Donkey anti-mouse A647	Thermo Fisher	ab150107	IF	1:400
Goat anti-mouse Star Green	Abberior GMBH	STGREEN-1001-50	IF-STED	1:100
Anti-rabbit HRP	Jackson Immunoresearch	711-035-152	WB	1:5000
Donkey anti-guinea pig HRP	Jackson Immunoresearch	706-035-148	WB	1:5000

IF, immunofluorescence; WB, western blotting; ChIP, chromatin immunoprecipitation